Analysis of giant resonances in proton, ^{3}He, and α scattering and the spin-flip strength in ^{208}Pb

H. P. Morsch and D. Cha
Institut für Kernphysik, Kernforschungsanlage Jülich, D-5170 Jülich, Federal Republic of Germany

J. Wambach
Department of Physics, University of Illinois, Urbana-Champaign, Illinois 61801

(Received 23 October 1984)

In an attempt to study isovector spin-flip excitations and to find a consistent picture of giant resonances in ^{208}Pb, we analyzed giant resonance data from 172 MeV α scattering, 140 MeV ^{3}He scattering, and 200 MeV proton scattering. Using spectroscopic information from α scattering, a good description of recent ^{3}He scattering data is obtained. A detailed analysis of results from different probes reveals differences between complex particle and proton spectra which are interpreted as due to spin-flip contributions. The spin-flip strength is estimated in a microscopic p-h model. At the scattering angles considered it gives resonant strength at $\sim$9 MeV dominated by 2^- excitations and further gives an increasing continuum yield towards higher excitation energies. The cross sections of these spin-flip excitations in (p,p′) are comparable to giant resonance yields and have to be considered in order to obtain a description consistent with complex particle spectra. The continuum part of isoscalar excitations is rather different from that of isovector spin-flip excitations. These features are qualitatively understood from the nuclear matter response. Calculations using the semi-infinite nuclear slab model of Esbensen and Bertsch give an almost quantitative description of isoscalar and spin-isospin continuum.

I. INTRODUCTION

Recently, there has been much interest in the investigation of collective spin-flip modes which are strongly excited by the hadronic force at bombarding energies of 200 MeV.[1] Most of the experimental information has been obtained so far from the (p,n) charge exchange reaction[2] in which the 1^+ Gamow-Teller (GT) resonance is the dominant feature in the 0° spectra, but also $L=1$ spin-flip excitations are clearly observed at larger neutron angles. In the inelastic (p,p′) reaction[3] collective 1^+ excitations have been identified in lighter nuclei up to the Zr region which complement information on $M1$ excitations from electron scattering[4] and resonance fluorescence.[5] For ^{208}Pb so far only a small amount of $M1$ strength is observed[6] including a 1^+ excitation at 5.8 MeV of mainly isoscalar structure.[7,8] Since in charge exchange and the inelastic channel different isospin components are strongly excited, it is of importance to study both types of reactions. Compared to the (p,n) reaction, in the inelastic channel the spin modes are shifted towards lower excitation energies; therefore the widths should be smaller. Of special interest are, aside from $M1$ strength, the dipole spin-flip modes excited by tensor operators of the type $[\sigma\tau Y_1]^{0^-,1^-,2^-}$. Especially the 2^- component is of great relevance for studying the energetic separation of spin current and convection current contributions of the electromagnetic distribution.[9] This separation has been discussed in connection with twist motion of the nucleus[10] indicating transverse zero sound propagation. Furthermore, the 2^- excitation is important in connection with neutronization processes of heavy nuclei during the gravitational collapse of super novae.[11]

To study isovector spin-flip excitations in the inelastic channel there is a large complication due to the fact that isoscalar non-spin-flip excitations are dominant. Because of this, in order to extract spin-flip strength a quantitative knowledge of the isoscalar response is absolutely necessary. Hence, such an investigation has to be embedded in a detailed analysis of isoscalar excitations observed in different hadron scattering experiments. Only if a consistent description of *all* the data from different probes is achieved can spin-flip information be obtained rather unambiguously. Sufficient data on giant resonances from different systems exist only for ^{208}Pb.

In the first part of the paper (Sec. II) a consistent analysis of different hadronic systems is discussed within the double folding approach. It is shown that the absolute strength of isoscalar excitations observed in p, d, ^{3}He, and α scattering can be described consistently. In some detail we consider the following: the properties of α and d scattering at 43 MeV/nucleon, 140 MeV ^{3}He scattering, and 200 MeV proton scattering from ^{208}Pb.

In the second part (Sec. III) a microscopic description of spin-flip excitations in ^{208}Pb is discussed which predicts appreciable cross sections for (p,p′). For consistency we also calculate cross sections for dipole spin-flip excitations in the (p,n) channel which are in good agreement with experimental data. The spin-flip excitations in (p,p′) are found to be quite comparable to the excitation of isoscalar giant resonances, as one might expect from the energy dependence of the Love-Franey T matrix.[1]

An attempt is made to separate experimentally the iso-

scalar non-spin-flip ($S=0,T=0$) and the isovector spin-flip ($S=1,T=1$) response by comparing (α,α') and (p,p') spectra. Apart from resonant contributions in the structures at 9 and 10 MeV the continuum features of isoscalar and spin-isospin contributions indicate a quite different behavior which can be well understood by the global features of the nuclear matter response.

II. ISOSCALAR GIANT RESONANCES EXCITED IN DIFFERENT HADRON SCATTERING SYSTEMS

Recent progress in our knowledge of giant resonances has been achieved[12] by investigating inelastic scattering with different projectiles, from protons up to α particles, and different incident energies from $\sim$100 to 800 MeV. To obtain more details about the structures involved, and in particular to test the reliability of the extracted results derived from different scattering systems, it is necessary to perform a consistent analysis of all the data. Further, in the description of the cross sections it is important to obtain absolute sum rule strengths which are similar for different scattering systems. This is generally not the case; e.g., in most giant resonance analyses the usual potential approach[13] has been used in which the inelastic form factor is given by derivatives of the optical potential. In this description, appreciably smaller sum rule strengths (up to factors of 2–3) are extracted from proton scattering[14,15] than from strongly absorbing probes like ^{3}He and α scattering. On the other hand, differences in the dynamics of the scattering by different projectiles can be well accounted for in the double folding approach based on a microscopic picture of the scattering process (see, e.g., Ref. 16). Therefore, a consistent description of the data should be performed within a microscopic framework.

There are recent data on giant resonances for ^{208}Pb from different scattering systems—proton, ^{3}He, and α scattering[14,15,17,18]—with conclusions which are not consistent. For instance, in an analysis of ^{3}He scattering[17] the importance of $L=4$ contributions in the region of the giant quadrupole resonance (GQR) was stressed. Possible $L=6$ strength which was crucial to describe α scattering,[16] and which has large effects on the extracted results, was not considered at all. This is also the case in a recent study of 200 MeV proton scattering.[15] Another problem is the $L=2$ strength in the GQR region (see Ref. 18) which was also extracted too low in the (^{3}He,^{3}He') analysis.[17]

A. DWBA calculations using folding form factors

The double differential cross section for inelastic scattering from a spin zero ground state is given in linear response by

$$\frac{d^2\sigma}{d\Omega\, dE}=-\left[\frac{\mu}{2\pi\hbar^2}\right]^2\frac{k_f}{k_i}\lim_{\eta\to 0}\frac{\mathrm{Im}}{\pi}\left\{\langle\,|\,T^+(E-H+E_0+i\eta)^{-1}T\,|\,\rangle-\frac{|\langle\,|\,T\,|\,\rangle|^2}{E-i\eta}\right\}, \tag{1}$$

where $\mathbf{k}_i$ and $\mathbf{k}_f$ are the three-momenta of the incident and scattered projectile and μ is the reduced mass. H denotes the full nuclear Hamiltonian and $|\,\rangle$ the exact ground state with energy E_0.

In DWBA the transition operator T is given by

$$T=\sum_{i=1}^{A}\int d\mathbf{r}_i\chi^{(-)*}(\mathbf{k}_f,\mathbf{r})V(\mathbf{r}-\mathbf{r}_i)\chi^{(+)}(\mathbf{k}_i,\mathbf{r})\,. \tag{2}$$

Here $\chi^{(\pm)}$ denote the distorted waves in the incident and scattering channel and V denotes the interaction between the projectile and a target nucleon. For complex projectiles V is replaced by the folded interaction

$$V_F(\mathbf{r}-\mathbf{r}_i)=\int dr_j\,\rho(r_j)V(\mathbf{r}+\mathbf{r}_j-\mathbf{r}_i)\,, \tag{3}$$

where $\rho(r_j)$ is the projectile density. In expression (2) exchange contributions are neglected.

In the following we present a consistent analysis of different scattering systems using results on strengths, energies, and widths of isoscalar resonances extracted from small angle α scattering.[18] In this analysis the collective model is used in which the propagator in (1) is given by

$$\langle N\,|\,(E-H+E_0+i\eta)^{-1}\,|\,N\rangle=\frac{\rho^{N*}\rho^N}{E-E_N+E_0+i\eta}\,, \tag{4}$$

where ρ^N is the collective model transition density for mode N. Generally the radial form of a surface derivative is used (details are discussed in Ref. 16). Results obtained by using these collective model transition densities show generally good agreement with those of microscopic random phase approximation (RPA) calculations.[16,19]

In the collective model approach we consider a nucleon-nucleon interaction of the general form

$$V(\mathbf{r}-\mathbf{r}_i)=[V_{00}+V_{01}(\tau\tau_i)+V_{10}(\sigma\sigma_i)+V_{11}(\sigma\sigma_i)(\tau\tau_i)]g(\mathbf{r}-\mathbf{r}_i)\,. \tag{5}$$

This interaction is strongly energy dependent.[1] For the complex particle scattering systems discussed ($E<50$ MeV/nucleon) the inelastic matrix elements are completely dominated by V_{00}. So, only pure isoscalar non-spin-flip ($S=0,T=0$) excitations are considered; this is exact for α scattering. The isovector spin-flip ($S=1,T=1$) interaction V_{11} is very strong in 200 MeV (p,p'); contributions due to this are discussed in Sec. III. Here, it should be mentioned that Eq. (5) contains only the central part of the nucleon-nucleon interaction and ignores spin-orbit and tensor terms. The latter are not important in small angle complex particle scattering. In (p,p') spin-orbit contributions may effect mainly non-spin-flip transitions at large scattering angles, whereas tensor contributions can be important for spin-flip excitations.

For the radial shape of the interaction (5) a Gaussian of 1.68 fm range was used which is well suited for the

TABLE I. Optical potentials used in the DWBA calculations (Refs. 14, 16, and 20). The units of the potential depths are MeV, those of the radii and diffusenesses fm.

System	V_0	r_0	a_0	W	r_w	a_w	V_{so}	W_{so}	r_{so}	a_{so}	r_c
$p+^{208}Pb$	19.649	1.223	0.736	18.134	1.213	0.829	2.065	−0.753	1.113	0.558	1.328
$^3He+^{208}Pb$	180.0	1.092	0.902	17.80	1.538	0.757					1.3
$\alpha+^{208}Pb$	155.0	1.282	0.677	23.26	1.478	0.733					1.3

description of different scattering systems (see, e.g., Ref. 16). The volume integral of V_{00} was 446 MeV fm^3 in the case $E \leq 50$ MeV/nucleon. Due to a large surface sensitivity the radial integration (2) depends to some extent on the optical potentials used. This effect can be compensated by adjusting the effective force to describe known transitions, e.g., the excitation of the low lying states. In our calculations the strength of V_{00} is adjusted to describe the data for the low lying 3^- state in ^{208}Pb ($E_x = 2.61$ MeV). Using a transition density of surface derivative form which describes the electromagnetic properties (see the discussion in Ref. 16) well, the ^3He scattering data are well described by increasing V_{00} by 10%. Optical potentials for the different scattering systems[14,16,20] are given in Table I. In the case of 200 MeV proton scattering we obtain a good description of the 3^- cross sections of Ref. 14 using a volume integral of V_{00} of 180 MeV fm^3. This is consistent with that of the optical potential in Table I (see also Ref. 18). However, this interaction is smaller than that by Love and Franey.[1]

Dynamical aspects of the different scattering systems are illustrated for the excitation of the GQR region in Figs. 1 and 2. A comparison of α and d scattering is made in Fig. 1; ^3He and proton scattering is compared in Fig. 2. Experimentally the angular distribution of the GQR is rather flat,[16,18] indicating a mixture of different L values. Also cross sections for different multipolarities with the sum rule strengths indicated are given in Figs. 1 and 2. In the comparison of α and d scattering in Fig. 1 a significant difference becomes apparent. In filling out the deep diffraction minima in the $L=2$ cross sections the $L=4$ component is very important in d scattering. On the other hand, in α scattering the diffraction patterns of $L=2$ and 4 contributions are in phase at larger angles.[16] It is clear that an additional strong $L=6$ component is required to understand the α scattering data.[16] This was further confirmed by the inclusion of small angle data[18] (Fig. 1). Nevertheless, in more recent investigations[15,17] $L=6$ contributions were not considered. Of course, in proton scattering (Fig. 2) experimental data do not exist beyond the second $L=2$ cross section maximum, so one is not so sensitive to high L yields. However, in ^3He scattering the data exist over a sufficiently large angular range.

In the experimentally best accessible angular range of 8°–15° for all systems the $L=2$ excitation is clearly dominant in (p,p′) below 10° (Fig. 2). Generally in (p,p′) the yields for lower L structures are more pronounced than for complex scattering systems. To compare (p,p′) to a rather similar dynamical situation of strong dominance of $L=2$ yield in α scattering one has to go to scattering angles as low as 4°. In both cases the extracted $L=2$ sum rule strength is comparably large.

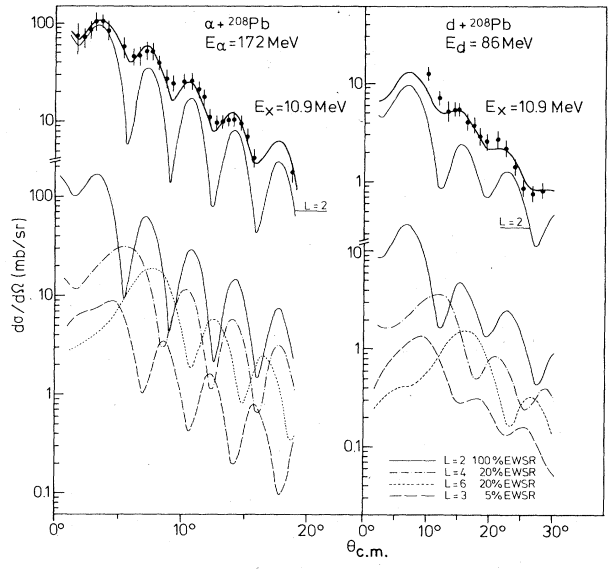

FIG. 1. Differential cross sections for the excitation of the GQR in ^{208}Pb in α and d scattering in comparison with DWBA calculations. Upper part: multipole excitation with the strength parameters in Table II (thick solid lines). The curves in the lower part correspond to calculations for $L=2$–6 with the sum rule strengths indicated. The data are from Refs. 16 and 18.

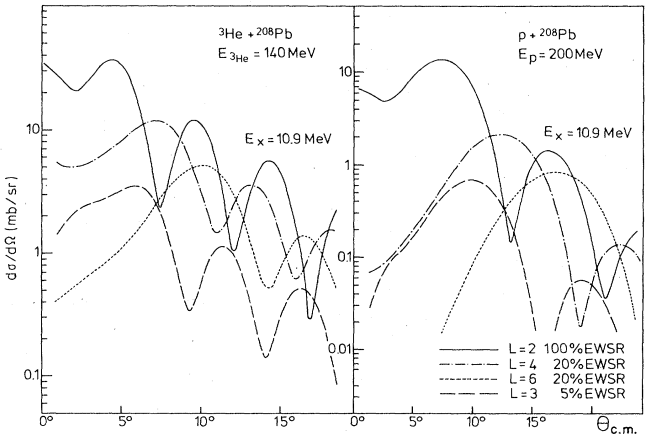

FIG. 2. Differential cross sections for ^3He and p scattering exciting different multipolarities in the region of the GQR with the sum rule strengths indicated.

TABLE II. Excitation strengths [in % of the energy weighted sum rule (EWSR)] of isoscalar giant resonance excitation.

	L	$\alpha+^{208}$Pb[a] 172 MeV	^{3}He$+^{208}$Pb[b] 140 MeV	p$+^{208}$Pb[c] 200 MeV
	2	59	59	53
GQR region	3	5	5	2
(10.9 MeV)	4	16	19	10(8)
	6	16	19	
12 MeV	4	14		14
structure	6			5
	0	90	90	90
GMR region	1	d	d	d
(13.8 MeV)	2	14	14	
	6	6	6	
16 MeV structure	6	15		
GOR (18.7 MeV)	3	60	(60—90)	
21.3 MeV	1	90		90[e]

[a]Sum rule strengths taken from Ref. 18.
[b]Background shape similar to α scattering (Ref. 18).
[c]Background shape different from α scattering.
[d]See Ref. 21.
[e]Reference 18.

B. Comparison with experimental results

In the following, giant resonance excitation in ^{3}He and proton scattering is discussed based on results obtained from α scattering. Giant resonance cross sections extracted from experimental data depend critically on the background shape assumed (see the discussion in Ref. 18). In the ^{3}He scattering analysis of Ref. 17 the background shape used is rather similar to that used in the study of α and d scattering.[16,18] In this case a direct comparison of results derived from α scattering with the ^{3}He scattering data of Ref. 17 is possible. The situation is quite different for 200 MeV proton scattering. Here, the multipole distribution in the giant resonance continuum is limited to lower L values. In addition, spin-flip contributions may give rise to significant contributions to the resonant and the continuum yield in (p,p'). Further, the isovector giant dipole resonance is strongly excited in 200 MeV proton scattering.[14] Cross sections for this excitation are calculated for the different systems as detailed in Ref. 21.

1. ^{3}He scattering

Differential cross sections for excitation of the 3^- state at 2.61 MeV, of the GQR (at 10.9 MeV), and of the giant monopole resonance (GMR), are given in Fig. 3; the data are taken from Ref. 17. The differential cross sections for the 3^- state are well described by our microscopic calculations. Using the multipole strengths (Table II) extracted from α scattering (Ref. 18, Table 1, fit 2) we obtain cross sections for GQR and GMR which are given by the dashed line for the GQR (10.9 MeV) and by the solid line for the GMR (13.7 MeV). A good agreement of our calculations with the experimental data is obtained; for the GMR we have a quantitative description of the absolute yields without any adjustment of the multipole strengths. For the GQR our calculations reproduce the overall trend of the data well; however, the absolute cross section is slightly underpredicted (the dashed line in Fig. 3). By adding a small component of higher multipolarity (3% $L=4$ and $L=6$), a good description of the data is obtained. The fact that somewhat smaller cross sections are predicted for the GQR from our α scattering data can be understood by a somewhat different background subtracted in the two different sets of data (which are, of course, analyzed completely independently). Nevertheless, the quantitative comparison in Table II shows clearly that giant resonance yields can be extracted reliably if a consistent description of several scattering systems is made. It has to be mentioned that the fits to the ^{3}He scattering data in Fig. 3 based on our α scattering results are much better than those given in Ref. 17. So, different from the conclusions drawn in Ref. 17, the data support our results of a strong $L=2$ excitation and the importance of $L=6$ contributions. A large $L=2$ strength in the range of the GQR (65% of the energy weighted sum rule strength) was also obtained in a recent (e,e'n) experiment of the University of Illinois group.[22]

2. Isoscalar excitations in proton scattering

The detailed comparison with giant resonance data obtained from high energy protons is more complicated. The first problem is a rather different structure of the background. In ^{3}He and α scattering the continuum background involves excitation of high multipolarity (up to $L\sim14$) at larger angles, whereas in the case of 200 MeV proton scattering only lower L values (up to ~6) contribute to the cross section in the measured angular region. Consequently, the angular distribution of the back-

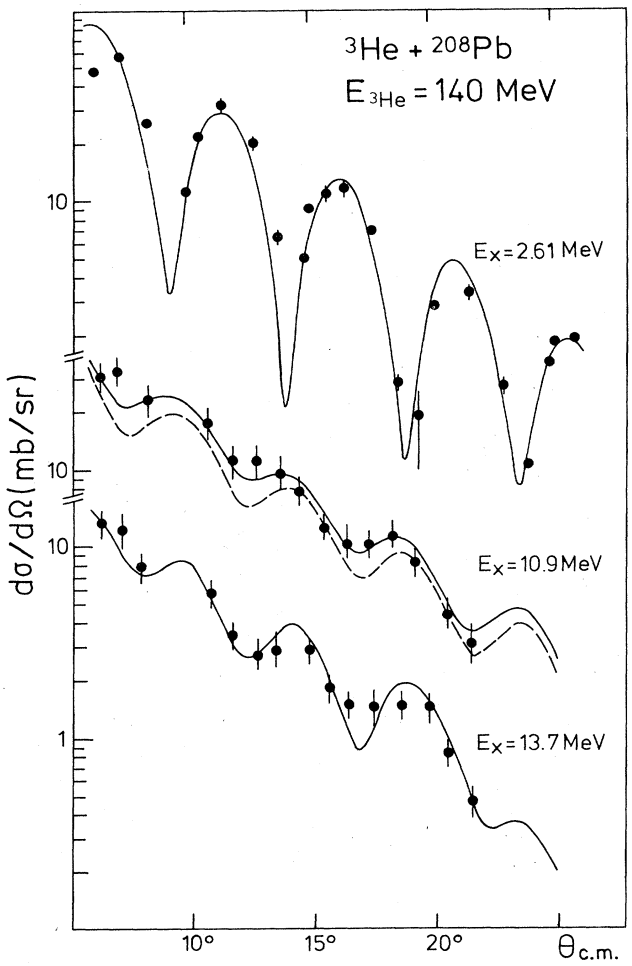

FIG. 3. Differential cross sections for excitation of the low lying 3^- state, the GQR, and GMR in ^{3}He scattering from ^{208}Pb in comparison with DWBA predictions with the sum rule strengths in Table II. The dashed line indicates a calculation with multipole strengths from α scattering. The data points are taken from Ref. 17.

ground can be rather different; possibly there is also an effect on the spectral shape.

In addition, there is the complication that also spin-isospin modes are strongly excited which give contributions to the background continuum and also to the resonant structure (this is discussed in Sec. III). Therefore it is not surprising that giant resonance parameters derived from complex particle spectra can be different from those obtained from 200 MeV proton scattering. An interesting example is the GQR in ^{208}Pb. Apart from indications for fine structure,[23] this resonance is well described in many hadron scattering systems by a Gaussian with $E_x \sim 10.9$ MeV and $\Gamma \sim 2.6$ MeV. Quite differently, in 200 MeV proton scattering[14] a double structure has been found in this region, one peak at 9.0 MeV with a width of 1.0 ± 0.1 MeV and the other at 10.6 MeV with a width of 2.0 ± 0.2 MeV. The 9 MeV peak observed in (p,p') may be identified mainly as part of the resonant spin-flip excitation (see Sec. III).

Differential cross sections for the GQR and the lowest 3^- state[14,15] are given in Fig. 4. The good description of the 3^- cross sections indicates that 200 MeV proton scattering data are well described by the microscopic DWBA approach (Sec. II A). The data for the GQR show the expected behavior discussed in Sec. II, namely that the first diffraction minimum of the $L=2$ distribution ($\sim 13°$) is smeared out by $L=4$ excitation. The differential cross sections are well described by $L=2$ and 4 excitations exhausting 53% and 10% of the corresponding isoscalar energy weighted sum rule (EWSR) strengths. Considering the uncertainties in the extracted background, the strengths are in good agreement with the α scattering results (Table II). Here, it should be noted that the smaller angle data of the GQR between 5° and 7° are not well described in these calculations. For the GQR an estimate of $L=6$ strength cannot be made since the data do not extend to large enough angles. The data extracted for the new structure at 12 MeV (Ref. 15) which are also included in Fig. 4 are well described by $L=4$ and 6 excitations with energy weighted sum rule strengths of 14% and 5%,

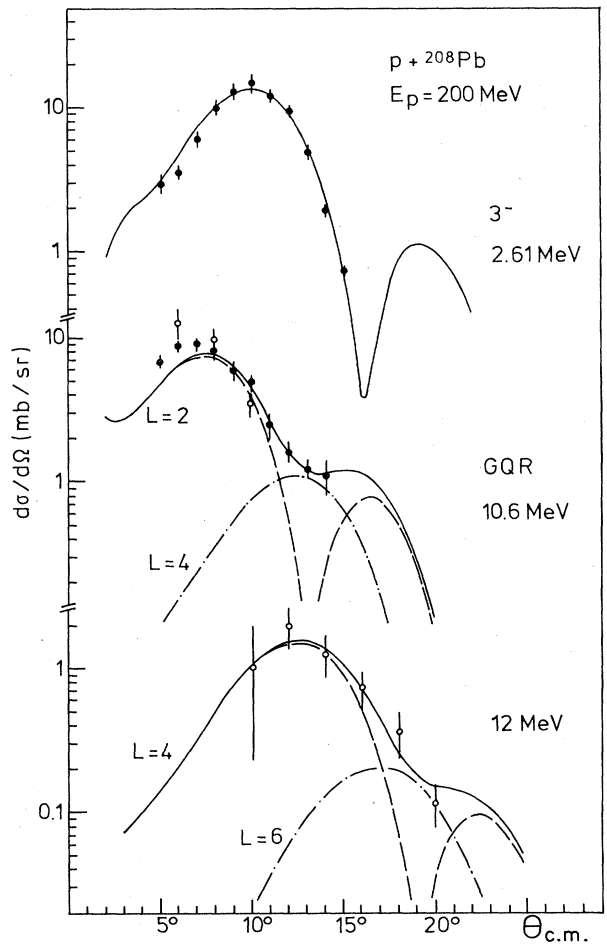

FIG. 4. Differential cross sections for excitation of the low lying 3^- state, the GQR, and the 12 MeV structure in ^{208}Pb in 200 MeV proton scattering in comparison with DWBA calculations with strengths in Table II. The data are taken from Ref. 14 (solid points) and Ref. 15 (open points).

respectively. The $L=4$ strength is in excellent agreement with that of the $L=4$ structure observed in α scattering.[18] The falloff of the cross section towards larger angles which is smaller than predicted by $L=4$ excitation may be a first indication for $L=6$ strength in proton scattering. In α scattering a much larger $L=6$ strength is found (see also Table II). The small evidence for $L=6$ excitation in proton scattering may be for the following reason: both $L=4$ and 6 excitations are strongly mixed in the $2\hbar\omega$ excitation region; apart from the concentrated $L=4$ structure at ~ 12 MeV the average ratio of EWSR strengths $S(L=4)/S(L=6)$ is about 0.4. This gives a rather flat angular distribution in the region between 10° and 18°, which may be subtracted in the spectra as part of the background. This would also explain that a smaller $L=4$ strength is derived from the GQR cross section in Fig. 4. These arguments are supported by the discussion of spectra in Sec. III C, indicating that in proton scattering a somewhat higher background is subtracted than in α scattering.

Concerning higher energetic giant resonances, the proton scattering data are consistent with α scattering. In the microscopic approach we obtain a quantitative description of the giant monopole (and isovector dipole) cross section and also an excellent description of the squeezing mode ($L=1, T=0$); the latter has already been discussed in Ref. 18.

III. SPIN-FLIP EXCITATIONS IN PROTON SCATTERING

The evidence for low energy spin-flip strength in ^{208}Pb is still a controversial question. Since ^{208}Pb is non-spin saturated we expect in the independent particle model (IPM) two strong 1^+ transitions: $\pi h\frac{11}{2}\rightarrow\pi h\frac{9}{2}$ and $\nu i\frac{13}{2}\rightarrow\nu i\frac{11}{2}$ with $B(M1)\uparrow$ values of 25.6 μ_N^2 and 22.1 μ_N^2, respectively. Some of this strength,[6] about 8.5 μ_N^2, i.e., 17.4% of the IPM value, has been seen between 7 and 8 MeV. Another tentative 8.5 μ_N^2 (Ref. 6) are located between 8 and 9.5 MeV, increasing the percentage of 35%. This 1^+ strength should also be excited in inelastic proton scattering at small scattering angles. As the scattering angle increases, higher multipoles than 1^+ will be excited, dominantly the dipole spin-flip resonance. This resonance has been clearly identified in 160 MeV (p,n) charge exchange. On the basis of a microscopic calculation which will be described below we argue that this spin-dipole resonance is also excited in 200 MeV (p,p').

A. Theoretical calculations of spin-flip excitations

To calculate the theoretical cross section we use an approximate form of the DWBA cross section for inelastic nucleon-nucleus scattering given in Eq. (1). The target is described by a second order ph propagator[24,25] which includes 1p1h and 2p2h excitations, and the projectile is described by plane waves and a distortion factor N_D.[26] In terms of the scattering angle θ, the initial and final three-momenta $\mathbf{k}_i$ and $\mathbf{k}_f$, and the reduced mass μ we therefore have for excitations to states of multipolarity J

$$\frac{d^2\sigma}{d\Omega\, dE}(\theta)=-\left[\frac{\mu}{2\pi\hbar^2}\right]^2\frac{k_f}{k_i}4\pi(2J+1)N_D(\theta)F\,, \tag{6a}$$

$$F=\lim_{\eta\to 0}\frac{\mathrm{Im}}{\pi}\left\{\sum_{\substack{\mathrm{ph}\\ \mathrm{p'h'}}} T^{*J}_{\mathrm{ph}}[E-A^J_{\mathrm{php'h'}}(E)+E_0+i\eta]^{-1}T^J_{\mathrm{p'h'}}\right\}\,, \tag{6b}$$

where the ph matrix A^J is specified in terms of the residual interaction V as

$$A^J_{\mathrm{php'h'}}(E)=(\epsilon_{\mathrm{p}}-\epsilon_{\mathrm{n}})\delta_{\mathrm{pp'}}\cdot\delta_{\mathrm{hh'}}+\left\langle(\mathrm{ph})^J\left|V+\sum_{\mathrm{2p2h}}\frac{V\,|\,(\mathrm{2p2h})^J\rangle\langle(\mathrm{2p2h})^J\,|\,V}{E-\epsilon_{\mathrm{2p2h}}+i\eta}\right|(\mathrm{p'h'})^J\right\rangle\,. \tag{7}$$

In PWBA the particle-hole matrix elements of the transition operator T are given by

$$T_{\mathrm{ph}}=\left\langle 0\left|\sum_{i=1}^{A}e^{i\mathbf{qr}}V(\mathbf{q})\right|\mathrm{ph}\right\rangle\,, \tag{8}$$

where V is the Fourier transform of the projectile-target nucleon interaction and q is the momentum transfer $|\,\mathbf{k}_f-\mathbf{k}_i\,|$.

In the calculation of $d^2\sigma/d\Omega\, dE$ we approximate both the residual interaction V in Eq. (2) as well as the coupling between the projectile and target as correlated $\pi+\rho$ meson exchange. This interaction is specified by[27]

$$V(\mathbf{q})=\int g(\mathbf{q}-\mathbf{k})[V_\pi(\mathbf{k})+V_\rho(\mathbf{k})]d^3k\,, \tag{9a}$$

$$g(\mathbf{q})=\delta(\mathbf{q})-1/(4\pi q^2)\delta(\,|\,\mathbf{q}\,|-q_c)\,, \tag{9b}$$

$$q_c=3.93\ \mathrm{fm}^{-1}\,,$$

$$V_\pi(\mathbf{k})=-\frac{4\pi f_\pi^2}{m_\pi^2}\left[\frac{\Lambda_\pi^2-m_\pi^2}{\Lambda_\pi^2+k^2}\right]^2\frac{(\boldsymbol{\sigma}\cdot\mathbf{k})(\boldsymbol{\sigma}'\cdot\mathbf{k})}{k^2+m_\pi^2}\boldsymbol{\tau}\cdot\boldsymbol{\tau}'\,, \tag{9c}$$

$$V_\rho(\mathbf{k})=-\frac{4\pi f_\rho^2}{m_\rho^2}\left[\frac{\Lambda_\rho^2-m_\rho^2}{\Lambda_\rho^2+k^2}\right]^2\frac{(\boldsymbol{\sigma}\times\mathbf{k})(\boldsymbol{\sigma}'\times\mathbf{k})}{k^2+m_\rho^2}\boldsymbol{\tau}\cdot\boldsymbol{\tau}'\,, \tag{9d}$$

$f_\pi^2=0.081$, $m_\pi=0.699\ \mathrm{fm}^{-1}$, $\Lambda_\pi=6\ \mathrm{fm}^{-1}$;

$f_\rho^2=4.86$, $m_\rho=3.9\ \mathrm{fm}^{-1}$, $\Lambda_\rho=10\ \mathrm{fm}^{-1}$;

and has been shown in Ref. 28 to give a quantitative

description of magnetic states. Also this interaction is a fair approximation to more realistic $\pm$ matrices.[29] In the present calculations for (p,p′) we ignore 1Δ1h effects.

The distortion factor N_D which enters Eq. (1) has been evaluated from a DWBA calculation with surface peaked collective model form factors (see Sec. II B) using relativistic kinematics:

$$N_D(\theta)=\left[\frac{d\sigma}{d\Omega}(\theta)\right]_{\mathrm{DWBA}}\Big/\left[\frac{d\sigma}{d\Omega}(\theta)\right]_{\mathrm{PWBA}}. \qquad (10)$$

For the GT excitation in the ^{208}Pb (p,n) reaction, the microscopic model (including also 1Δ1h mixing[28]) gives 54% of the $3(N-Z)$ sum rule, which is in good agreement with the experimental results.[2] Also, the centroid energy and width are consistent with the data.

As a further test of the model we calculated the spin-dipole cross sections in the 160 MeV (p,n) reaction. In the lower part of Fig. 5 we show the yields in a 1p1h model [without the V^2 term in Eq. (7)]. These results are in good agreement with earlier RPA calculations. The effect of 2p2h mixing is very strong; the full calculations (including 1Δ1h mixing) is given in the upper part of Fig. 5. The various multipole contributions indicate that the peak in the energy distribution is dominated by 2^- excitation whereas the 1^- and 0^- yields are strongly damped. The second order contributions to the ph interaction increase the repulsion of the ph force pushing the strength to higher energies, a region of high level density. This push

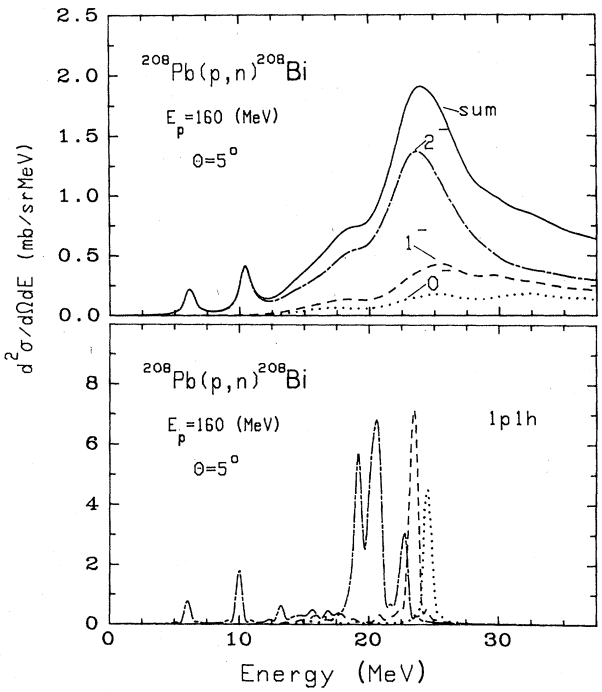

FIG. 5. Spectra computed for dipole spin-flip modes $(0^-,1^-,2^-)$ excited in the (p,n) reaction at 160 MeV at an angle of 5°. In the lower part results are given in a 1p1h calculation consistent with the calculations in Ref. 30. An energy averaging parameter η of 0.5 MeV was used in these calculations.

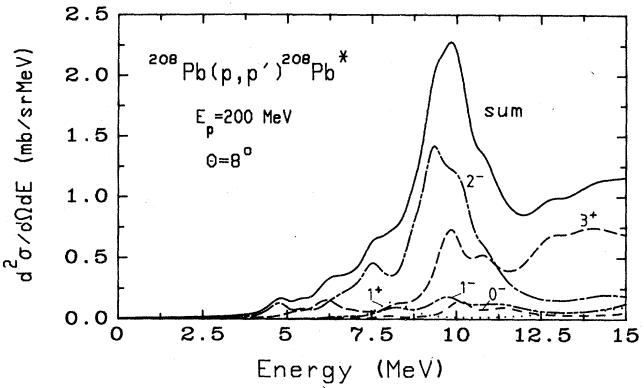

FIG. 6. Spectra computed for isovector spin-flip excitations in 200 MeV (p,p′) at a scattering angle of 8°.

is multipole dependent and strongest for 0^- and 1^- states. Therefore, the damping of 0^- and 1^- strength is larger than for 2^- excitations. The agreement with experiment is surprisingly good. The integrated strength between 0 and 40 MeV is 26.2 mb/sr as compared to 32 mb/sr found experimentally.

These results give us confidence that also the prediction for (p,p′) in Fig. 6 should be reasonable. For dipole spin-flip excitations $(0^-,1^-,2^-)$ rather similar features are obtained as found for (p,n), i.e., a strong bump due to 2^- excitation and rather damped 1^- and 0^- yields. In addition

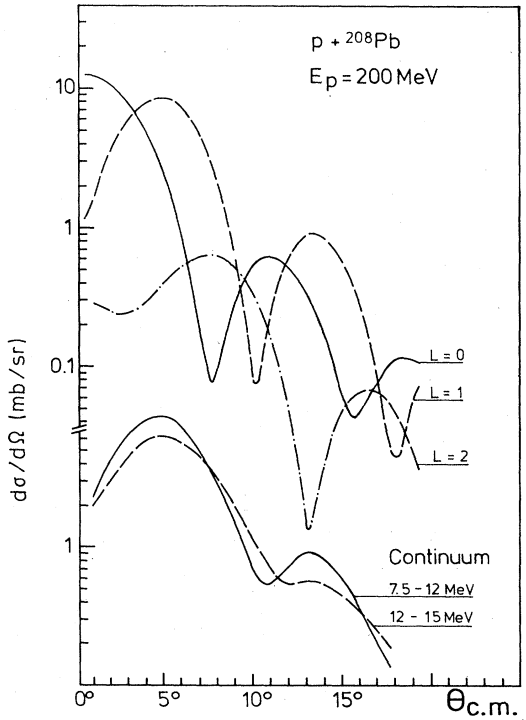

FIG. 7. Differential cross sections for spin-isospin excitations in 200 MeV (p,p′). In the upper part the different multipole components are shown for the resonant part (see the discussion in the text); the continuum contributions in two energy regions are given in the lower part.

to the spin dipole in Fig. 6 we have also included the 1^+ (dotted line) which, however, has minimal cross sections at $\theta=8°$, and further, the 3^+ excitation which is quite strong above 8 MeV. The energy location of the main peaks is consistent with earlier 1p1h RPA calculations of Ref. 9. Comparing our calculations to more refined calculations including 1Δ1h contributions and ground state correlations,[28] our strength is too large by about 30—40%. Furthermore, these correlations somewhat lower the centroid energies.

The total spin-flip strength in Fig. 6 may be divided into a resonant part below 10 MeV and a rising continuum part. Using a linear separation below 12 MeV differential cross sections are given in Fig. 7. For the resonant part the different L contributions are given; at very small scattering angles the 1^+ cross section is quite large. For the continuum part all multipolarities are added; the two curves given for different energy bins indicate that the angle dependence of the continuum is small.

B. Experimental evidence for spin-flip excitations in ^{208}Pb

The results of the calculations in Sec. III A have indicated that spin-flip excitations in 200 MeV proton scattering are quite comparable to those of isoscalar excitations in Figs. 2 and 4. If this is true, then one should be able to detect significant differences between proton scattering and α scattering (in α scattering spin-flip strength is absent). In Fig. 8 a comparison is made between a proton spectrum (Ref. 15) and a spectrum from 172 MeV α scattering, both spectra taken at scattering angles corresponding to the first maximum of the $L=2$ angular distribution ($q\sim0.45$ fm^{-1}). In these spectra there are marked differences in the resonant strength as well as in the continuum background, both taken from Refs. 15 and 18.

In the resonant strength there are differences in the region of the new high lying resonances[31] as well as in the lower region of the GQR. At high excitation energies in the α spectrum at 4° only the giant octupole resonance (GOR) is observed ($E_x=18.7$ MeV) (Ref. 32), whereas both the GOR and isoscalar dipole resonance[31] ($E_x=21.3$ MeV) should be excited in proton scattering. This may be seen by the shift of the high-lying structure to higher excitations in (p,p′).

Differences between (p,p′) and (α,α′) are found also in the region of the GQR. In complex particle scattering the GQR is described by a resonance at 10.9 MeV with a width of about 2.6 MeV.[16–18] However, as mentioned in Sec. II B, there is fine structure mainly on the low energy side of the GQR dominated by an $L=3$ excitation at 9.3 MeV which is clearly seen in the spectrum in Fig. 8. In proton scattering the location of the GQR is generally lower with also a smaller width of 2 MeV.[14,15] Actually, in the work of Ref. 14 the GQR region is fitted by two resonances, a resonance at 10.6 MeV with a width of 2 MeV and one at 9 MeV with a width of 1 MeV. The latter structure should not be identified with the 9.3 MeV peak seen, e.g., in α scattering: The 9.3 MeV structure in (α,α′) has an angular distribution[18] consistent with $L=3$, whereas the 9 MeV peak shows a rather different angular dependence (Fig. 9). In the proton spectrum of Ref. 15 displayed in Fig. 8 instead of one structure at 9 MeV, two resonances are indicated. None of these, however, is identical to the structure seen in the α spectrum in Fig. 8 at about 7.8 MeV which corresponds to the $L=4$ structures ($E_x=7.4$ and 8.1) studied earlier.[16] These are expected to be very weakly excited in small angle proton scattering and should not contribute much to the structure in the proton spectrum in Fig. 8.

The 9 MeV structure in (p,p′) may be interpreted as being of dominant spin-flip structure. Further, inconsistencies of resonance parameters for the GQR extracted from complex particle and proton scattering may also indicate that spin-flip components are also important in this resonance. In Fig. 9 differential cross sections for these two resonances are given; the data are taken from Ref. 14. These data can be well described taking into account the resonant spin-flip strength discussed in Sec. III A: For the GQR for which the small angle data in Fig. 4 were not well described by the pure $L=2$ and 4 fit a quantitative description is obtained by adding about a quarter of the predicted resonant ($L=1,S=1$) strength (the $L=4$ strength is slightly reduced to 8% of the EWSR). The ad-

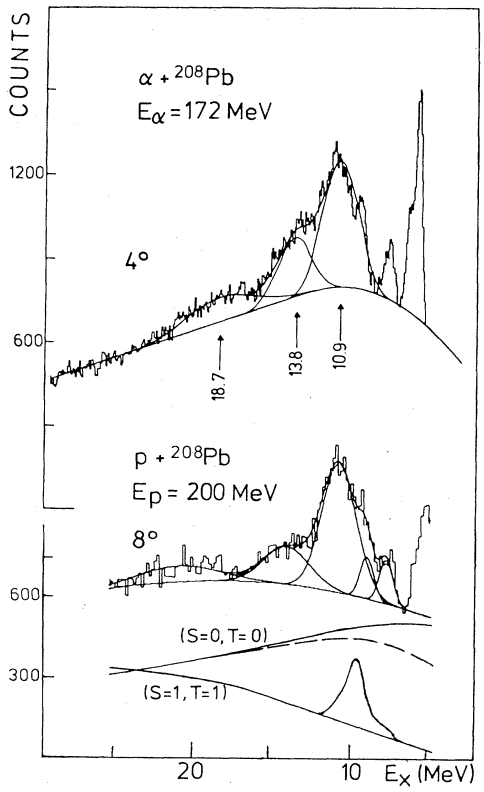

FIG. 8. Comparison of α and proton spectra at scattering angles corresponding to the first maximum of the $L=2$ angular distribution ($q\sim0.45$ fm^{-1}). The data as well as resonance and background fits are taken from Refs. 15 and 18. For proton scattering the calculated spin-isospin response ($S=1,T=1$) is given as well as the extracted isoscalar response ($S=0,T=0$) (see the text).

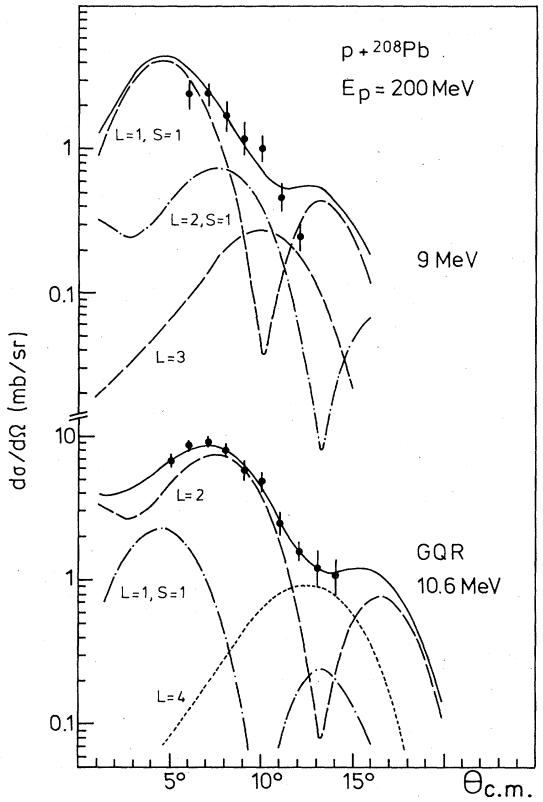

FIG. 9. Differential cross sections for the excitation of the 9 and 10.6 MeV structures in (p,p') in comparison with DWBA calculations including spin-flip contributions. The data points are from Ref. 14.

dition of $L=1$ strength can explain the somewhat lower centroid energy and width of the GQR in (p,p'). The 9 MeV cross section in Fig. 9 can be fitted by a mixture of $(L=1,S=1)$, $(L=2,S=1)$, and a small fraction of $L=3$ strength (2% EWSR) reminiscent of the isoscalar $L=3$ structure at 9.3 MeV.[16,18,23] In this fit the whole $(L=2,S=1)$ strength is assumed and 43% of the predicted $(L=1,S=1)$ strength. Adding the dipole yield in the GQR cross section we obtain 67% of the resonant dipole spin-flip strength (Fig. 7). This is in excellent agreement with our predictions in Sec. III A if one realizes that Δ quenching and ground state correlations have not been included in our calculations; this can give a quenching of the dipole spin flip yield[28] on the order of 30—40%. In spite of this good agreement it has to be mentioned that the fit to the 9 MeV structure in Fig. 9 is not really convincing. The angular distribution could be described as well by a dominant $L=2$ shape. This shows that more detailed data, in particular at smaller angles, have to be taken before the spin-flip strength in this structure is well established.

The largest differences in the spectra of α and proton scattering are in the shape of the background continuum. In α scattering it falls off to larger excitations, whereas it stays rather constant in proton scattering. From the preceding discussion we expect that this difference may be due to spin-flip strength. To estimate the dominant isoscalar $(S=0,T=0)$ and spin-isospin $(S=1,T=1)$ contributions to the continuum one may subtract the spin-flip strength in Sec. III A (Fig. 6) from the experimental background. Separated into resonant and continuum contributions, the spin-flip strength is plotted in the lower part of Fig. 8. Subtracting the continuum from the experimental background yields the solid line indicated $(S=0,T=0)$. On the other hand, we may take the isoscalar continuum from the α spectrum. Adjusting the height at the highest excitations in the same way as before yields the dashed line which is rather similar to the solid line. Of course, one has to realize that it is not at all clear whether the $(S=0,T=0)$ continuum in α scattering can be directly compared to that in proton scattering. We know, e.g., that the dynamics of small L compression modes is very different in the two scattering systems. On the other hand, we expect that the dynamical features of the dominant surface response are not so different for both cases, so that the subtraction technique appears to be more or less justified for higher excitations and small angles.

These results indicate that isoscalar and isovector parts of the inelastic continuum can be separated with properties which are dramatically different: The spin-isospin continuum is strongly quenched at low excitation but overshoots the isoscalar continuum at high energies. These features can be well understood by global properties of the nuclear response discussed in the next subsection.

C. Properties of the continuum response in a nuclear matter approach

In the preceding discussion we have seen that under certain assumptions the comparison of spectra (see Fig. 8) gives direct information on different spin-isospin channels, in our case mainly on $(S=0,T=0)$ and $(S=1,T=1)$ modes. Both of these types of excitations have resonant and continuum parts. The resonant parts are dominated by low L structures yielding detailed information on the shell model structure of the nucleus and the properties of damping mechanisms. On the other hand, in the continuum part excitations of many different (higher) multipolarities are present which have comparatively large spreading. It is clear that these continuum excitations probe important aspects of the nuclear response; this may be seen by the large differences of isoscalar and spin-isospin continua in Fig. 8.

In the following an attempt is made to identify the nuclear continuum by the global response of infinite or semi-infinite nuclear matter (see also Ref. 33). In the Fermi gas model the double differential cross section per effective number of nucleons is given in PWBA by

$$\frac{d^2\sigma}{d\Omega\, dE}(q)/\text{nucleon} = -\,\text{Im}\left[\left[\frac{m_N}{2\pi\hbar^2}\right]^2 \frac{k_f}{k_i}\frac{3\pi}{k_F^3}\sum_{ST}|V_{ST}(q)|^2\Pi^0_{ST}(q,E)\right], \tag{11}$$

where m_N is the nucleon mass, k_i and k_f are the magnitudes of initial and final three-momenta of the scattered projectile, and q is the momentum transfer. $V_{ST}(q)$ denotes the interaction between projectile and target nucleon in the various channels (S,T) and $\Pi^0_{ST}(q,E)$ is the free polarization propagator.[34] Choosing values close to the Love-Franey t matrix, $V_{00}=-150$ MeV fm^3, $V_{01}=80$ MeV fm^3, $V_{10}=30$ MeV fm^3, and $V_{11}=170$ MeV fm^3, we obtain the cross section denoted by the dashed line in Fig. 10. The Fermi momentum k_F has been chosen somewhat lower than the nuclear matter value corresponding to about 70% of nuclear matter density, which is more appropriate for ^{208}Pb.

The free Fermi gas response is modified by the ph correlations. For repulsive interactions the response is quenched and for attractive interactions the response is enhanced.[35] In RPA Π^0_{ST} has to be replaced by the interacting propagator given by

$$\Pi_{ST}(q,E)=\Pi^0_{ST}(q,E)/[1-V^{ph}_{ST}(q)\Pi^0_{ST}(q,E)] . \quad (12)$$

Taking the parameters of the ph interaction V^{ph}_{ST} from Landau-Migdal theory[36] fitted to nuclear excited states, $V^{ph}_{00}(q)=-50$ MeV fm^3, $V^{ph}_{01}(q)=210$ MeV fm^3, $V^{ph}_{10}(q)=0$ MeV fm^3, and $V^{ph}_{11}(q)=150$ MeV fm^3, we obtain the results denoted by the two full lines in Fig. 10. Since the isoscalar interaction V^{ph}_{00} is attractive, the strength is shifted to lower energies. In contrast, the isovector response is shifted to higher energies since both V^{ph}_{01} and V^{ph}_{11} are repulsive. The bulk of the isovector cross section is spin-flip $(S=1,T=1)$; the $(S=0,T=1)$ contribution, which is rather small, is indicated by the dashed-dotted line. These results are in good agreement with the results in Ref. 35 and show the right qualitative features of the differences between isoscalar and isovector continua seen experimentally (Fig. 8).

A more realistic treatment in the same spirit uses semi-infinite nuclear matter including surface dynamics.[37] This allows for a more quantitative comparison with experiment when solved in RPA similar to (12). In this approach the response is pushed significantly to lower excitation energy due to the surface effects (Fig. 11). The comparison with our experimental results taken from Fig. 8 clearly shows that the main features are well reproduced. The absolute cross sections are described quantitatively. Only the response is pushed a bit too much to the low excitation region. However, in comparison with the data in Fig. 11, one should realize that quite large isoscalar strength is above the "background" at low excitation, filling up part of the yield between the shaded area and the solid line in Fig. 11.

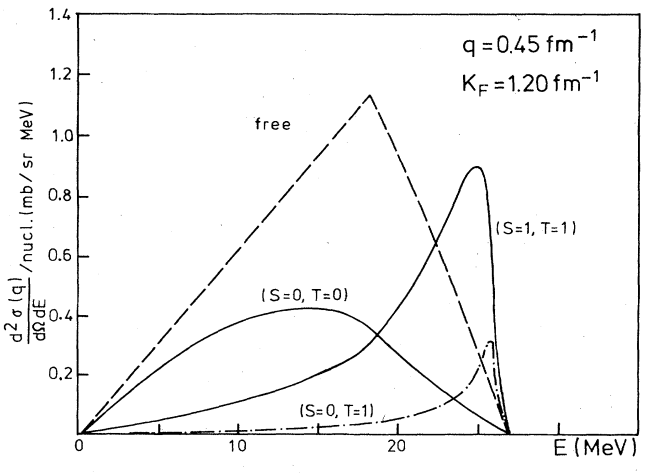

FIG. 10. Nuclear matter estimate of the inelastic response in (p,p'). The dashed line shows the free Fermi gas model prediction whereas the other lines take into account the attractive $(S=0,T=0)$ and the repulsive $(S=0,T=1)$ and $(S=1,T=1)$ parts of the nuclear force.

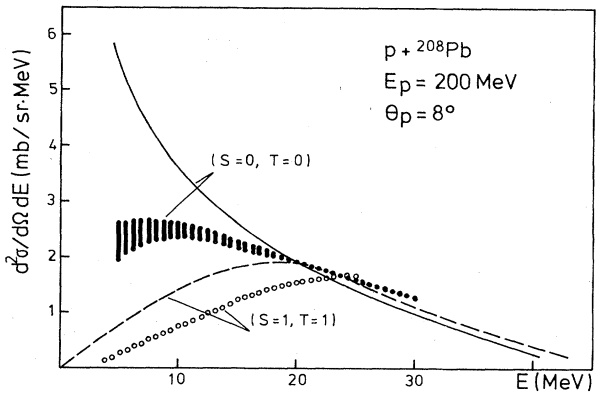

FIG. 11. Continuum part of the isoscalar $(S=0,T=0)$ and spin-isospin $(S=1,T=1)$ response—solid bars and open points, respectively—taken from the results in Fig. 8 in comparison with calculations using the semi-infinite nuclear matter model of Esbensen and Bertsch (Ref. 37) (solid and dashed lines).

That the absolute yields are well described for 200 MeV proton scattering is of large importance (see also Ref. 33). It indicates that the nuclear interaction, in particular the isoscalar force V_{00}, is weak enough at 200 MeV, so that the data are described by a single scattering process (this is assumed in the formalism discussed in Secs. II A and III A). For 172 MeV α scattering this approximation is not justified for excitation of the continuum. Here the strength of the force V_{00} is about twice as much, so multiple excitations become important. Indeed, using the same model of Esbensen and Bertsch[37] for the description of α scattering, only about one-third of the continuum yield is obtained; this result is similar to a continuum estimate based on a partial wave expansion (Ref. 12).

IV. SUMMARY

In this paper different aspects of excitation of giant resonances and magnetic structures in ^{208}Pb have been studied. A main emphasis was put on a consistent and complete analysis of isoscalar giant resonances observed in different scattering systems. This has been achieved within a folding model description. By using consistent background shapes giant resonance yields in the scattering of different probes can be quantitatively compared, with rather small uncertainties in the EWSR strengths.

A second emphasis was placed on the understanding of spin-isospin modes which may be detected by comparison

of proton scattering and α scattering. First, microscopic calculations have been presented which describe the different spin modes (GT and spin-dipole) in the (p,n) charge exchange reaction well. These calculations indicate significant spin-flip strength in the (p,p') channel with cross sections quite comparable to those of isoscalar excitations. In the comparison of α and proton scattering the structure observed at about 9 MeV can be well understood by spin-flip excitations in excellent agreement with our predicted strength. It is clear that out results have to be confirmed in more detailed small angle scattering experiments.

The continuum features of the isoscalar and spin-isospin response were found to show very dramatic differences which can be understood by the global properties of the nuclear matter response. It is important to note that a quantitative description of the background and its properties is possible for 200 MeV proton scattering. On the other hand, the application of the single scattering approximation to the α scattering continuum yields only one-third of the experimental yield, indicating that multiple excitations are important in this case. Under particular dynamical conditions, e.g., in heavy ion reactions with large GQR cross sections, multiple collisions may give rise to new effects, e.g., multiple phonon excitation of the GQR producing new structures not seen in light ion scattering. An example for this may be the structures seen in Ref. 38.

ACKNOWLEDGMENTS

The authors are indebted to H. Esbensen and G. F. Bertsch for valuable discussion concerning continuum calculations and a prompt provision of the calculations presented in Fig. 11. Further, critical discussion of giant resonance details with F. E. Bertrand is acknowledged.

[1]W. G. Love and M. A. Franey, J. Phys. (Paris) **C4**, 231 (1984).
[2]C. Gaarde, J. Rapaport, T. W. Taddeucci, C. D. Goodman, C. C. Foster, D. E. Bainum, C. A. Goulding, M. B. Greenfield, D. J. Horen, and E. Sugarbaker, Nucl. Phys. **A369**, 258 (1981); C. Gaarde, *ibid.* **A396**, 127c (1983).
[3]N. Anantaraman, G. M. Crawley, A. Galonsky, C. Djalali, N. Marty, M. Morlet, A. Willis, and J. C. Jourdain, Phys. Rev. Lett. **46**, 1318 (1981); C. Djalali, J. Phys. (Paris) **C4**, 375 (1984).
[4]A. Richter, Nucl. Phys. **A374**, 177c (1982), and references therein.
[5]U. E. P. Berg, J. Phys. (Paris) **C4**, 359 (1984).
[6]G. E. Brown and S. Raman, Comments Nucl. Part. Phys. **9**, 79 (1980).
[7]K. Wienhard, K. Ackermann, K. Bangert, U. E. P. Berg, C. Bläsing, W. Naatz, A. Ruckelshausen, D. Rück, R. K. M. Schneider, and R. Stock, Phys. Rev. Lett. **49**, 18 (1982).
[8]S. I. Hayakawa, M. Fujiwara, S. Imanishi, Y. Fujita, I. Katayama, S. Morinobu, T. Yamazaki, T. Itahashi, and H. Ikegami, Phys. Rev. Lett. **49**, 1624 (1982).
[9]D. Cha and J. Speth, Phys. Rev. C **29**, 636 (1984).
[10]G. Holzwarth and G. Eckart, Z. Phys. A **283**, 219 (1977).
[11]J. Cooperstein and J. Wambach, Nucl. Phys. **A420**, 591 (1984).
[12]H. P. Morsch, J. Phys. (Paris) **C4**, 185 (1984).
[13]See, e.g., G. R. Satchler, Phys. Lett. **39B**, 495 (1972).
[14]C. Djalali, N. Marty, M. Morlet, and A. Willis, Nucl. Phys. **A380**, 42 (1982).
[15]J. R. Tinsley, D. K. McDaniels, J. Lisantti, L. W. Swenson, R. Liljestrand, D. M. Drake, F. E. Bertrand, E. E. Gross, D. J. Horen, and T. P. Sjoreen, Phys. Rev. C **28**, 1417 (1983).
[16]H. P. Morsch, C. Sükösd, M. Rogge, P. Turek, and C. Mayer-Böricke, Phys. Rev. C **22**, 489 (1980).
[17]T. Yamagata, S. Kishimoto, K. Iwamoto, K. Yuasa, M. Tanaka, S. Nakayama, T. Fukuda, M. Inoue, M. Fujiwara, Y. Fujita, I. Miura, and H. Ogata, Phys. Lett. **123B**, 169 (1983).
[18]H. P. Morsch, P. Decowski, M. Rogge, P. Turek, L. Zemło, S. A. Martin, G. P. A. Berg, W. Hürlimann, J. Meissburger, and J. G. M. Römer, Phys. Rev. C **28**, 1947 (1983).
[19]J. Wambach, thesis, Kernforschungsanlage Jülich, 1979 (unpublished); J. Speth and J. Wambach, Nucl. Phys. **A347**, 389 (1980).
[20]A. Djaloeis, J. P. Didelez, A. Galonsky, and W. Oelert, Nucl. Phys. **A306**, 221 (1978).
[21]P. Decowski and H. P. Morsch, Nucl. Phys. **A377**, 261 (1982).
[22]G. O. Bolme, L. S. Cardman, R. W. Doerfler, L. J. Koester, B. L. Miller, C. W. Papanicolas, and S. E. Williamson, University of Illinois report, 1984 (unpublished).
[23]H. P. Morsch, P. Decowski, and W. Benenson, Nucl. Phys. **A297**, 317 (1978).
[24]A. M. Lane, *Nuclear Theory* (Benjamin, Amsterdam, 1964); C. Yannouleas, M. Dworzecka, and J. J. Griffin, Nucl. Phys. **A397**, 239 (1983).
[25]B. Schwesinger and J. Wambach, Phys. Lett. **134B**, 29 (1984).
[26]F. Petrovich, in *The (p,n) Reaction and the Nucleon-Nucleon Force,* edited by C. D. Goodman *et al.* (Plenum, New York, 1980), p. 115.
[27]G. E. Brown, J. Speth, and J. Wambach, Phys. Rev. Lett. **46**, 1057 (1981).
[28]D. Cha, B. Schwesinger, J. Wambach, and J. Speth, Nucl. Phys. **A430**, 321 (1984).
[29]W. G. Love, M. A. Franey, and F. Petrovich, in *Spin Excitations in Nuclei,* edited by F. Petrovich *et al.* (Plenum, New York, 1984), p. 205.
[30]F. Osterfeld, S. Krewald, H. Dermawan, and J. Speth, Phys. Lett. **105B**, 257 (1981).
[31]H. P. Morsch, M. Rogge, P. Turek, and C. Mayer-Böricke, Phys. Rev. Lett. **45**, 337 (1980).
[32]H. P. Morsch, M. Rogge, P. Turek, P. Decowski, L. Zemło, C. Mayer-Böricke, S. A. Martin, G. P. A. Berg, I. Katayama, J. Meissburger, J. G. M. Römer, J. Reich, P. Wucherer, and W. Bräutigam, Phys. Lett. **119B**, 311 (1982).
[33]G. F. Bertsch and O. Scholten, Phys. Rev. C **25**, 804 (1982).
[34]A. L. Fetter and J. D. Walecka, *Quantum Theory of Many Particle Systems* (McGraw-Hill, New York, 1971).
[35]W. M. Alberico, A. Molinari, R. Cenni, and M. B. Johnson, Ann. Phys. (N.Y.) **138**, 178 (1982).
[36]A. B. Migdal, *Theory of Finite Fermi Systems and Applications to Atomic Nuclei* (Wiley, New York, 1967), Interscience Vol. 19, Scripta Technica.
[37]H. Esbensen and G. F. Bertsch, Ann. Phys. (N. Y.) **157**, 255 (1984).
[38]Ph. Chomaz, N. Frascaria, Y. Blumenfeld, J. P. Garron, J. C. Jacmart, J. C. Roynette, W. Bohne, A. Gamp, W. von Oertzen, M. Buenerd, D. Lebrun, and Ph. Martin, Z. Phys. A **318**, 41 (1984).